Hindawi
Advances in Civil Engineering
Volume 2020, Article ID 8836505, 20 pages
https://doi.org/10.1155/2020/8836505

Research Article

Experimental Study on the Transverse Effective Bending Rigidity of Segmental Lining Structures

Yong-feng Tang,[1] Han-cheng Chen,[1] Zhen-wei Ye,[1] Ting-jin Liu ,[2,3,4] and Yu-bing Yang [5]

[1]*School of Civil Engineering and Transportation, South China University of Technology, Guangzhou 510640, Guangdong, China*
[2]*South China Institute of Geotechnical Engineering, South China University of Technology, Guangzhou 510640, Guangdong, China*
[3]*State Key Laboratory of Subtropical Building Science, South China University of Technology, Guangzhou 510640, Guangdong, China*
[4]*School of Engineering, University of Tasmania, Hobart 7005, Tasmania, Australia*
[5]*College of Water Conservancy and Civil Engineering, South China Agricultural University, Guangzhou 510642, Guangdong, China*

Correspondence should be addressed to Ting-jin Liu; liu_tingjin@163.com

Received 6 September 2020; Revised 13 November 2020; Accepted 24 November 2020; Published 10 December 2020

Academic Editor: Wen-Chieh Cheng

The transverse effective rigidity ratio is a key parameter when the uniform rigidity ring model is adopted to design or numerically analyse segmental lining structures commonly used on a shield-driven tunnel. Traditionally, the transverse effective rigidity ratio η is treated as a constant, which can be evaluated through theoretical analysis and model tests. In this study, scale models were designed and tested to investigate the variation of the transverse effective rigidity ratio in the segmental linings' flattening deformation process. The test results suggested that in the elastic stage, the transverse effective rigidity ratio fluctuated between 0.667 and 0.734 for the stagger-jointed rings and fluctuated between 0.503 and 0.642 for the straight-jointed rings. When segmental linings were squashed and started to crack at the circumferential joints, the transverse effective rigidity ratio decreases sharply. Then, a regression equation was obtained to fit the variation trend of η with the increase of horizontal convergence to the outer-diameter ratio ($\Delta D/D_{out}$). Finally, in a case study, the regression equation was adapted to determine the value of η of an operated shield tunnel which was once surcharged accidentally and deformed severely so as to numerically predict the prospective deformation induced by the upcoming adjacent excavation. Numerical results indicated that as the value of η decreases, the horizontal convergences of shield tunnel induced by adjacent excavation increase significantly and even more than doubled in the case study. Comparatively, through taking account of the operating tunnels' exiting transverse deformation, the predicted deformation tends to be unfavourable.

1. Introduction

The shield-driven tunnelling method has been widely used for the construction of underground tunnels in urban areas because it has advantages including flexibility, highly safe construction efficiency, and minimum impact on the surrounding environment. Most shield-driven tunnels have utilised segmental linings connected by steel bolts. Besides, tunnel segments are often articulated or coupled at longitudinal and circumferential joints. Therefore, the characteristics of joints have a notable influence on the behaviour of the segmental linings. As a result, the effect of the joints on internal forces and deformation characteristic should be taken into consideration in the design or safety evaluation of the tunnel lining. In the engineering and numerical analyses related to the underground shield-driven tunnel problems, figuring out accurately the mechanism performance of segmental linings has always been one of the major foci [1–3].

Consequently, appropriate design models, which can accurately reflect the internal force and the loading

condition imposed by the various surrounding ground, are essentially required. In 1978, the International Tunnelling Association [4] set up a professional team to collect design model for shield tunnel linings applied in different countries. Lee et al. [5] classified the typical methods of shield tunnel lining design into four major categories: (a) empirical design methods based on past tunnelling practices; (b) design methods based on the in situ measurement and laboratory testing; (c) circular ring in elastic foundation method; and (d) continuum mechanics models including analytical methods and numerical methods.

Generally, shield tunnel lining behaviour is often approached as two plane problems along the transverse and longitudinal direction in the design process although it is a three-dimensional problem [6, 7]. Accordingly, the shield tunnel lining is usually regarded as a planar problem in the transverse direction. Among the design models mentioned above, more often than not, the circular ring in the elastic foundation method is utilised for both design and analysis purposes. This method can also be categorized according to how the joints of concrete segments are regarded, namely: (1) uniform rigidity ring method [8]; (2) average uniform rigidity ring [9–12]; (3) multihinge ring [13]; and (4) beam-spring model [14–16]. The structural models that correspond to these approaches are illustrated in Figure 1.

The uniform rigidity ring method is carried out by absolutely ignoring the existence of the segment joints and that resulting in an inaccurate bending moment at the joint area. The multihinge ring method takes the segment joints as perfect pins and is suitable and appropriate for the tunnelling boring machine- (TBM-) driven tunnel in hard rock [17], where the surrounding rock can maintain self-stability and transfer enough reaction to the lining. The beam-spring model, which simulates segmental joints with rotational springs and reflects relatively accurate stiffness of the segmental joints, is comparatively complex in calculation and limited in application. In fact, after a great number of practices and experience, especially in soft ground, the average uniform rigidity ring method has been widely employed in segmental lining design of shield tunnel for its clear mechanical concept and the simple calculation. In the average uniform rigidity ring method, the presence of the joints is considered by introducing two factors [12], namely, the effective ratio of bending rigidity η reflecting the relative stiffness between the segmental lining and the continuous lining structure and the transfer ratio of bending moment ξ reflecting the relative stiffness between segment and joint. Accordingly, the equivalent stiffness of the segmental ling ring is ηEI ($\eta \leq 1$), as shown in Figure 2, and the bending moments of the segment and the joint are modified to be $(1 + \xi)\ M_0$ and $(1 - \xi)\ M_0$, respectively, as shown in Figure 3.

Thus, it can be seen that the value of the effective ratio of the transverse bending rigidity has great theoretical significance because the maximum bending moment of segments and the diameter convergence of linings are closely associated with the effective rigidity. Until now, the research studies mainly focus on the value and influence of the effective ratio of the transverse bending rigidity, typically by the means of analytical solution and laboratory structural testing.

Wood [10] presented an analytical approach to compute the effective ratio of the transverse bending rigidity taking the influence of joint stiffness and segment number into consideration. Through assuming the deformation mode of the circular tunnel is an ellipse, Liu and Hou [19] proposed the elastic analytical formula for the value of η of the segmental lining. Lee et al. [5] proposed the iterative analytical method of η through employing the multihinge ring model, and the fitting formula of the relationship between the effective ratio of the transverse bending rigidity and the parameters (tunnel radius, lining thickness, strata resistance coefficient, joint stiffness ratio, etc.) was obtained for the segment assembling types with the straight joint. Accordingly, their research concluded that the value of η ranges from 0.1~0.6 in most of the soft ground. Zhong et al. [20] qualitatively analysed the effective ratio of the transverse bending rigidity after comparing the results calculated by the average uniform rigidity ring and beam-spring models. Also, they suggested that the effective ratio of the transverse bending rigidity η of Chinese subway tunnels generally ranges from 0.4 to 0.8.

Xu [21] and Huang et al. [22] fabricated the segments and joints with polyethylene (PE) and PE sheets separately and assembled into two-ring tunnel models. The laboratory model test result indicated that the effective rigidity ratios of the tunnel with straight joints and stagger joints were 0.67 and 0.75, respectively, for Shanghai Metro and the effect of soil resistance on the effective rigidity of shield tunnel was very small in soft ground. Ye et al. [23] designed and manufactured three types of circular ring model, namely, straight-jointed ring, stagger-jointed ring, and uniform ring, which were made of PMMA simulating segments and aluminium welding wire simulating bolts. It is reported that the range of the effective ratio of the transverse bending rigidity value is between 0.09 and 0.23 under straight-jointed condition and 0.30 and 0.80 under stagger-jointed condition. Zheng et al. [24] also adopted polyethylene and aluminium wire to fabricate the shield tunnel models, and the effective rigidity ratios of the tunnel were investigated through testing the model under the concentrated load and realistic loading pattern in sandy soil. Taking the Shanghai Yan-Jiang Tunnel as an example, Li et al. [25] analysed the influence of buried depth on the effective ratio of the transverse bending rigidity and found that the buried depth has a great influence on η. Feng et al. [26] carried out prototype tests on segmental lining structure for shield tunnel with a large cross section and attained the variation pattern of η and ξ with load conditions; the experiment also showed that as the section increases, η increases while ξ decreases. Many Japanese scholars suggested that the method of the whole ring loading test should be used to determine η. In the design of Tokyo Bay expressway shield tunnel, Uchida [27] adopted the uniform circular ring model with $\eta = 0.8$ and then carried out the prototype loading test of the whole ring to prove the reasonability and validity of the value. Kashima et al. [28] conducted prototype loading tests on the stagger-jointed mode of the DPLEX shield tunnel and determined that an η value of 0.8 was meaningful. In conclusion, Japan Society of Civil Engineers recommends

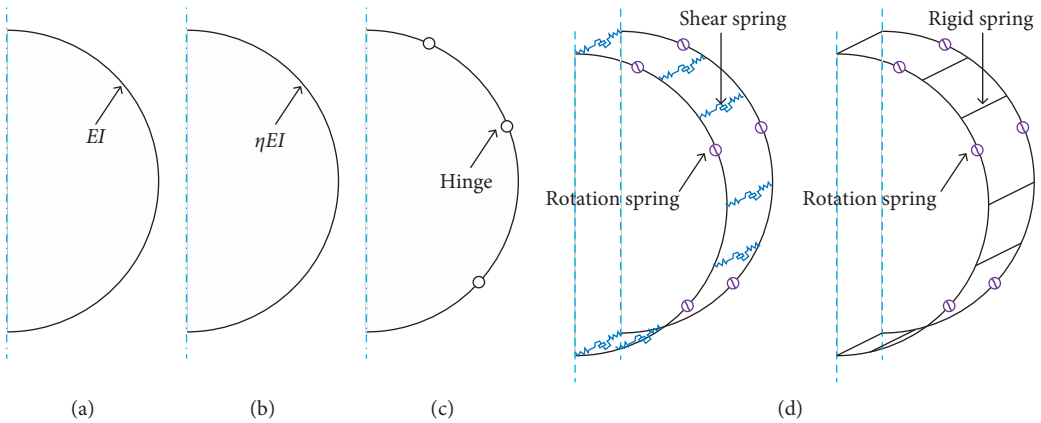

Figure 1: Structural models of the shield segment. (a) Uniform rigidity ring method. (b) Average uniform rigidity ring. (c) Multihinge ring. (d) Beam-spring model.

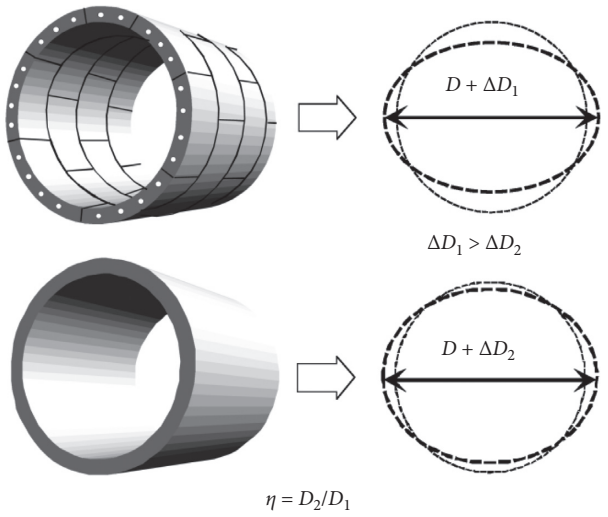

Figure 2: Concept of the effective ratio of bending rigidity [11].

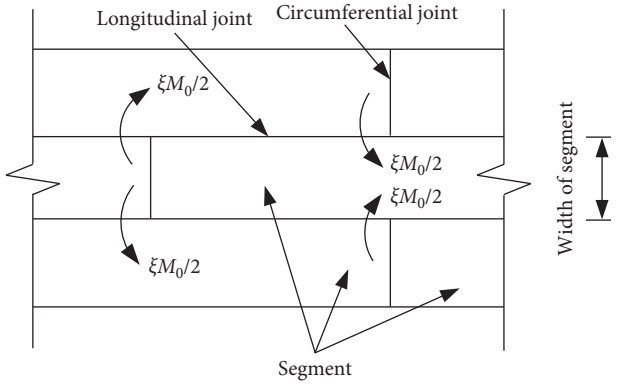

Figure 3: Transferring of bending moment between adjacent rings [18].

values of η and ζ of 0.8 and 0.3, respectively. At present, model tests are still the mainstream method to investigate the effective ratio of the transverse bending rigidity.

It is common to treat the segmental linings as a continuous ring with a discounted rigidity in the numerical analyses related to the shield tunnel. For instance, Chen et al. [1] set the effective rigidity ratios of the lining for circumferential directions to be 0.7 in order to numerically investigate the influence of large excavation on tunnel. Zheng et al. [29] performed finite element analyses to investigate the effect of cutoff wall on protecting the tunnel from deformation. And the transverse effective rigidity ratio of tunnel lining was also set to 0.7.

Previous studies mainly focus on the transverse effective bending rigidity ratio in the elastic stage. For example, elastic materials are always used in model tests [22–24]. However, the damage process of the material of segment rings as the load increases can also conversely influence the value of the transverse effective bending rigidity ratio. In this paper, lining structure model tests, which are fabricated by brittle gypsum material rather than the conventional elastic polymer materials, are first carried out to investigate the transverse effective bending rigidity ratio in the whole process of loading. Second, a regression equation is developed to reflect the variation trend of η with the increase of diameter convergence based on the experimental results. Third, for numerical modelling purposes, a practical method is suggested to determine the value of η based on the existing horizontal deformation of an operated shield-driven tunnel that can be obtained from on-site measurement.

2. Physical Model Tests

2.1. The Similarity of Model Tests. Physical models need to satisfy a variety of similarity relationships in terms of geometry and physical-mechanical properties so that the conclusions of the model can represent the prototype. The similar model test is based on the model similarity theory, which has three common points that can guide the design of the model test and the processing of test data. In the model test, the segmental tunnel linings used in Guangzhou city are taken as the prototype.

The geometric similarity ratio $C_l = 20$ and elastic modulus $C_E = 20$ are chosen as basic similarity ratios. The weights of segmental rings are not considered because of their negligible impact compared to those caused by the overburden pressure and the ground overload. Accordingly, a series of similarity ratio between the prototype parameters and the model parameters can be deduced, including the similarity ratio of displacement $C_\delta = C_l = 20$, stress $C_\sigma = C_E = 20$, rotation $C_\theta = C_l = 1$, and strain $C_\varepsilon = C_\delta / C_l = 1$.

2.2. Modelling of the Segment. Figure 4 shows a typical shield tunnel cross section with an outer diameter of 6 m and an inner diameter of 5.4 m. The segmental lining is composed of a universal segment combination of three standard segments, i.e., B1, B2, and B3, two counter key segments, i.e., L1 and L2, and one key segment, F. The width of the segmental lining is 1.5 m. Adjacent segments are connected with two circumferential M24 curve bolts, and adjacent segmental rings are connected with ten longitudinal M24 curve bolts.

The strength grade of the concrete used for the segmental linings is C50 in Chinese concrete code. For the purpose of simulating the concrete effectively, the segmental lining model is made of a mixture of gypsum with diatomite and water, which has similar brittleness and failure mechanics to that of concrete [30] In this experiment, a number of proportioning tests and compressive strength tests were performed until the mechanical parameters can meet the requirements. The final proportion in the mixture is gypsum : diatomite : water = 1 : 0.3 : 1. Figure 5 shows one of the compressive strength tests of the gypsum specimen. In addition, the circumferential reinforcement and longitudinal reinforcement of prototype concrete segments are of HRB400E grade, the elastic modulus of which is 210 GPa. But the detailing reinforcement of concrete segments is ignored for its little effect on the lining models' overall performance. After comparing the mechanical property of a variety of metal wires, the tinned iron wire whose elastic modulus is 165 GPa is chosen to simulate the reinforcement of concrete segments. According to the equivalent principle of tensile rigidity, the diameter of the tinned wire distributed in the inner and outer cambered surface of segments is 0.5 mm and 0.6 mm, respectively, and the spacing of the double layer tinned wire is equally 35 mm both in the inner and outer cambered surfaces of segments. Meanwhile, the diameter of the longitudinal wire is 0.4 mm and the spacing is 30 mm. The longitudinal wires and circumferential wires were welded into wire mesh, as shown in Figure 6. Table 1 provides the geometrical parameters and material property of the segmental lining.

2.3. Modelling of the Circumferential Joints. The circumferential joints influence the segmental linings' overall behaviour seriously, but the complicated structural characteristics of joints bring great difficulties to their simulation. In fact, the compression stiffness and shear stiffness of circumferential joints have little influence on the internal force and deformation of the segmental lining, and it is feasible to only consider the bending stiffness. Usually, as the segmental lining is under the external load and deformed, joints at different positions will open inward or outward. Therefore, the inner and outer dividing groove method is used to simulate the circumferential joints [31–33]. In the segmental lining models, the dividing grooves with a certain width and depth were cut at the locations corresponding to the circumferential joints. The detailed structure of the circumferential joint of shield tunnel is shown in Figure 7, and the circumferential joint of the segmental lining is regarded as an articulation with a certain bending rigidity. In the experiment, the simplified method of the equal absolute value of bending stiffness under positive and negative bending moment is used to simulate the segment joint, although the bending rigidity of positive and negative bending moment is not the same. The bending stiffness of the groove must meet the requirements of similarity ratio. According to the research findings [5], the value of the bending rigidity of circumferential joint can be approximately 5×10^4 kN·m/rad, so the width and depth of the groove are calculated by using formulas (1) and (2) developed in [32]. Generally, it is recommended that the central angle of the groove is 3°~5° for the accuracy of the simulation and the convenience of fabricating. Finally, both of the groove width and depth are coincidentally determined to be 5 mm.

$$H_1 = \sqrt[3]{\frac{12 L_1 k I}{b(EI + kL)}} = \sqrt[3]{\frac{12 I k \alpha (D_1 + D_2)}{2bEI + bk\alpha l (D_1 + D_2)}}, \quad (1)$$

$$H = \frac{((t - H_1)/C_L)}{2}, \quad (2)$$

where H_1 and L_1 represent the width and depth of the groove based on prototype segmental lining, respectively, H represents the depth of the groove based on the scaled model, k represents the rotational stiffness of the prototype circumferential joint, E and I represent the elastic modulus and area moment of inertia of the prototype segment respectively, b represents the width of the prototype segment, D_1 and D_2 represent the external diameter and the internal diameter of the prototype segment, and α represents the central angle of the groove.

2.4. Modelling of the Longitudinal Joints. To simulate the boundary condition, the three-ring segmental lining structure was assembled by longitudinal joints for testing. Guo et al. [34] and Wang et al. [33] considered the stiffness of the longitudinal joint which was large enough to be assumed as infinite, and simplistically, the straight steel bars were used to simulate the joints between segmental rings in their experiment. To be more exact, the stiffness between segmental rings is finite and relative deformation, for example, joint opening and dislocation will occur commonly in actual projects. Also, the shear force possibly varied in different assembly modes, and that is why straight-jointed and stagger-jointed rings have obviously different deformation characteristic. Therefore, the

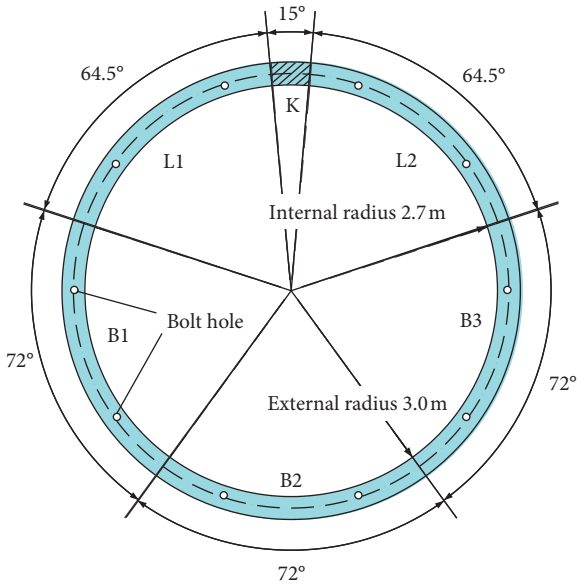

Figure 4: Cross section of the segmental lining.

Figure 5: Compressive strength tests of the gypsum specimen.

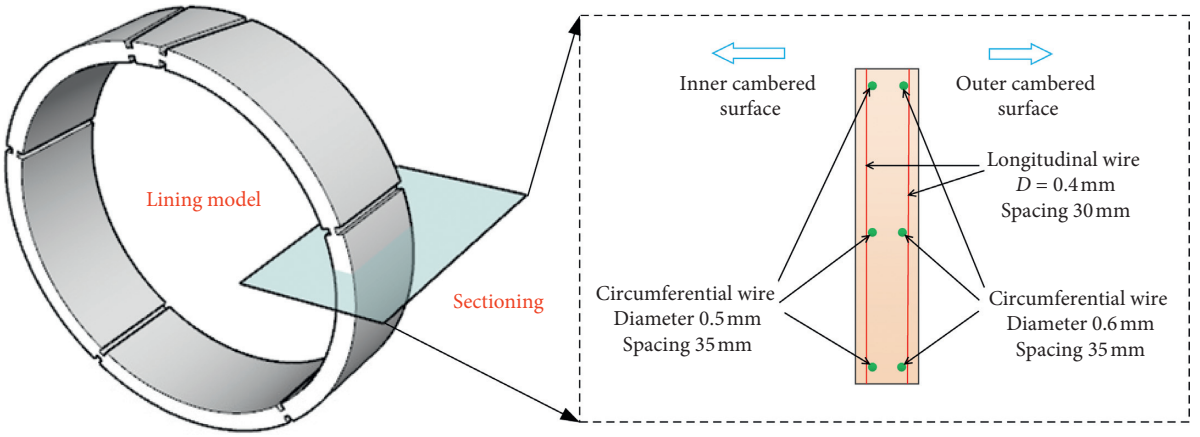

Figure 6: Distribution of the segment reinforcements.

longitudinal bolts are considered as elastic spring and the stiffness relationship between the prototype and the model is expressed by

$$\left(\frac{nE_bA_b}{l_b}\right)_p = \left(\frac{nE_bA_b}{l_b}\right)_m C_E C_L^2, \tag{3}$$

Table 1: Mechanical and geometrical parameters of the model tunnel.

Parameters	Relation	Prototype	Model
Inner diameter (mm)	$C_d = C_l = 20$	2700	135
Thickness of the segmental lining (mm)	$C_t = C_l = 20$	300	15
Width of the segmental lining (mm)	$C_w = C_l = 20$	1500	75
Elastic modulus of the segmental lining (GPa)	$C_E = 20$	35.5	1.83
Compressive strength of the segmental lining (MPa)	$C_R = C_E = 20$	59.8	3.3
Total tensile stiffness of the reinforcement in the inner cambered surface of segments (kN)	$C_{EA} = C_E C_l^2 = 8000$	938700	140
Total tensile stiffness of the reinforcement in the outer cambered surface of segments (kN)	$C_{EA} = C_E C_l^2 = 8000$	551460	97

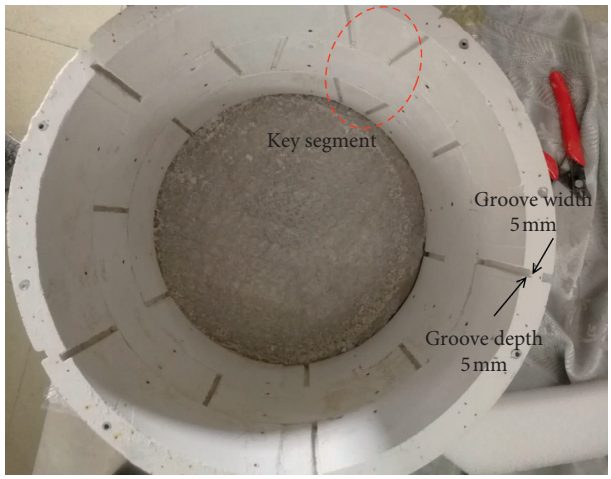

Figure 7: Circumferential joint processing diagram.

where n is the number of longitudinal bolts, E_b is the elastic modulus of bolts, A_b is the area of a single bolt, and l_b is the length of bolts.

The material selection of longitudinal bolts can be determined based on the similarity ratio requirement and the manufacturing requirements; several materials including aluminium welding wires, iron wires, and brass wires were taken as samples for testing. The tensile result shows that the elastic modulus of the aluminium welding wire (type 1060) is 2.45×10^4 MPa, and it is suitable to be bent into the needed shape for its flexibility. Thus, we decided to select aluminium welding wire to simulate bolts and calculate the diameter and length of aluminium welding wire using equation (3). The geometric and mechanical properties of longitudinal bolts of model and prototype segmental lining are shown in Table 2.

2.5. Model Fabrication. The fabrication process involves many steps. First of all, a handmade and detachable mould was designed and manufactured for the casting of segmental linings. The handmade mould was mainly made up of two thin aluminium sheets and several circular wooden boards. When assembling the mould, the two thin aluminium sheets were rolled into cylinders, the diameter of which was the inner and outer diameters of the segmental lining model, respectively, and the wooden boards are used to support and keep the shape of the aluminium sheets. Also, the double layer wire mesh (simulating reinforcement), rubber strips (forming circumferential dividing grooves), and hollow aluminium tubes (forming longitudinal bolt holes) were positioned precisely and embedded inside the mould in advance. Next, the gypsum mixture was poured into the mould, forming multiple ring model, as shown in Figure 8. Then, the multiple ring model was cut into single rings according to the width of the segmental linings, and the embedded hollow aluminium tubes were simultaneously cut in half. Finally, the single rings were assembled into three-ring segmental linings through longitudinal joints.

Figure 9 shows the details of the longitudinal joints. After cutting out the single rings, the aforementioned aluminium welding wires (simulating longitudinal bolts) pass through the bolt hole formed by the hollow aluminium tubes. Both ends of longitudinal bolts were fixed by fixators, and the pretension force of longitudinal bolts was applied so that the adjacent rings were assembled firmly.

2.6. Apparatus of Model Tests and Experimental Procedure. Figure 10 shows the overall view of the apparatus of the model loading test. The model tests were conducted through the load structure method on a specially designed experimental bench. According to the research proposed by Huang et al. [22], the transverse effective rigidity ratio of segmental linings in the soft ground (the typical ground resistance coefficient is 10000 kN/m^3) is almost the same as that of segmental linings without lateral confinement. Therefore, the lateral confinement was not imposed in the test. The segmental rings were supported on the experimental bench, and the line load was applied by a loading box at vault position of linings. There were two rubber strips sticking on both sides of contact line between the segmental lining and the experimental bench. Through the rubber strips, the displacement of the segmental lining's bottom was constrained, and the physical model's rigid-body displacement and rotation were in turn constrained. Also, four vertical rods were installed to ensure that the loading box only has the freedom of vertical movement, and then the line load can be applied exactly at vault position of segmental lining.

Since the weight of the loading box was 1.6 kg approximately, placing the loading box on the top of the segmental lining was regarded as the first loading stage. Then, each subsequent loading was applied through placing standard weights (1.5 kg) into the loading box. The loading was applied step by step until the segmental linings were destroyed.

The middle ring among the assembled three-ring segmental linings was the target ring to be measured. To reveal the

Table 2: The geometric and mechanical properties of model and prototype segmental lining.

Type	Elastic modulus (MPa)	Length of bolt (mm)	Diameter of bolt (mm)	Longitudinal bolt number
Prototype	2.06×10^5	470	24	10
Model	2.45×10^4	31.8	0.9	10

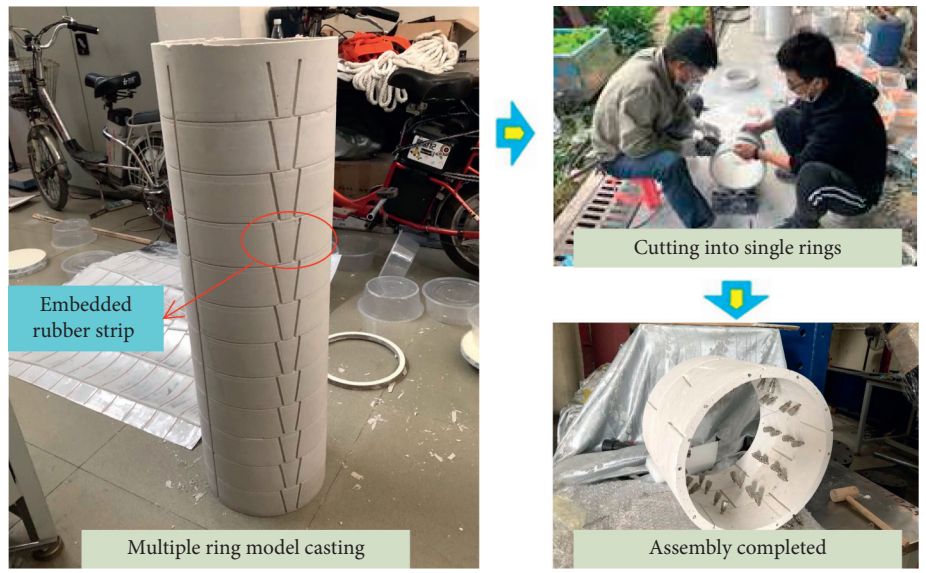

Figure 8: Brief fabrication process of segmental linings.

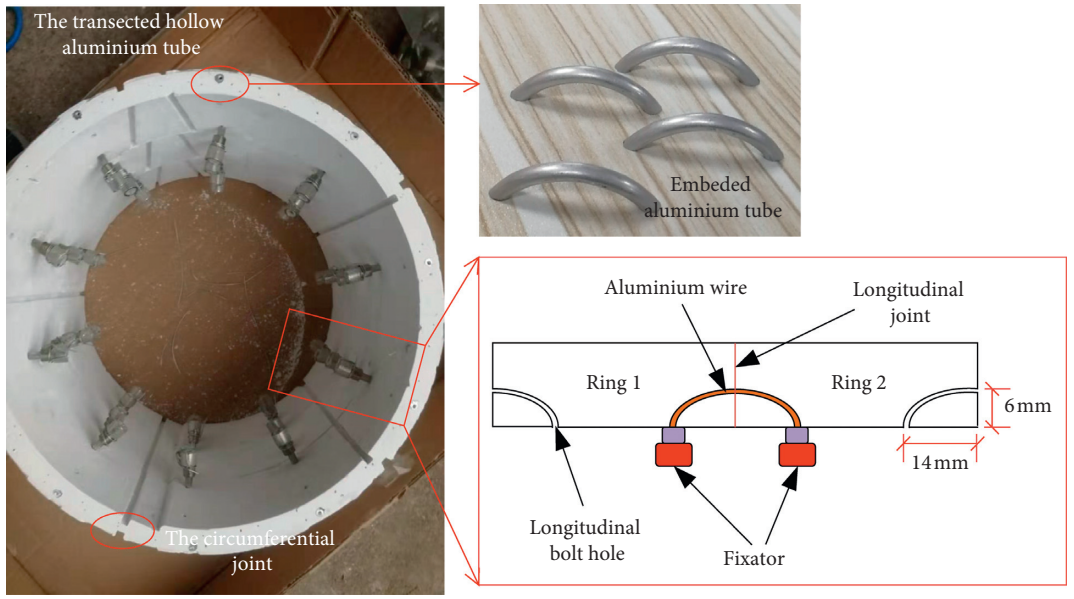

Figure 9: The details of the longitudinal joints.

radial deformation of the target ring effectively, digital micrometres and static data collecting gauge were used to measure and collect the displacement during the test. Eight digital micrometres were distributed symmetrically around the circular direction at an equal angle interval of 45 degrees, and an extra digital micrometre was used to monitor the possible movement of the experimental bench. A diagrammatic sketch of the arrangement of the devices is shown in Figure 11.

2.7. Grouping and Test Content. To investigate the deformation characteristic of segmental linings under different assembled conditions, three types of segmental linings in different assembled modes were tested, including uniform ring (only longitudinal joint), straight-jointed rings, and stagger-jointed rings, which are shown in Figure 12. Besides, the key blocks of the straight-jointed rings and the stagger-jointed rings are located at the vault and the vault offset of 18°.

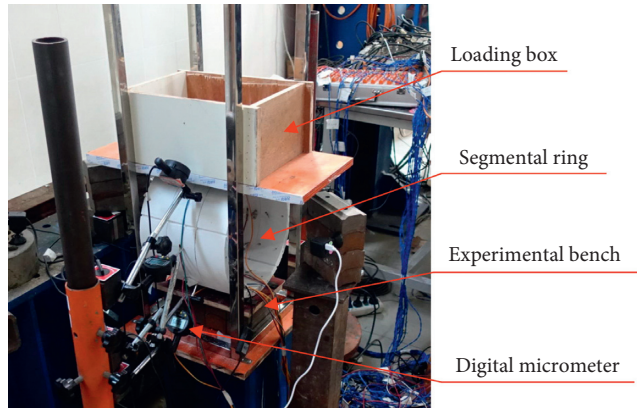

Figure 10: Apparatus of model loading test.

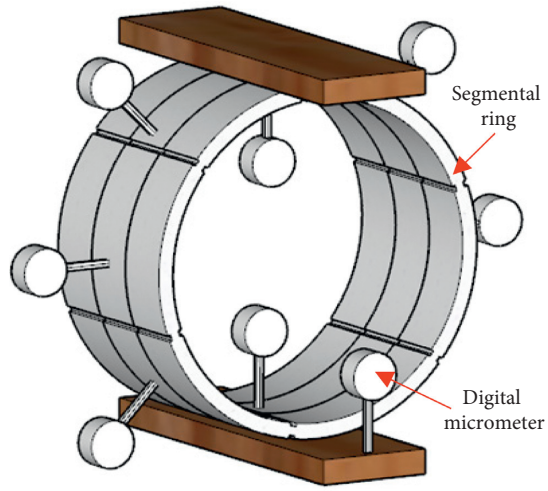

Figure 11: Arrangement of the measurement devices.

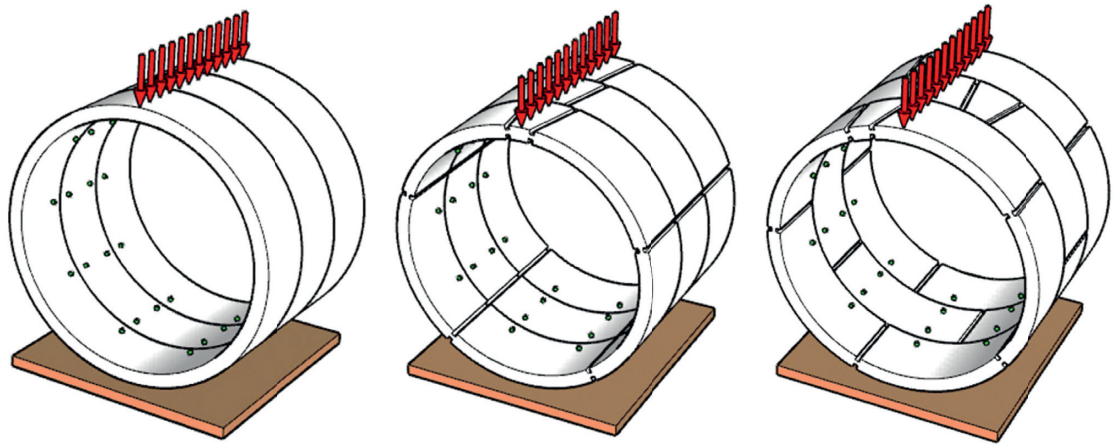

Figure 12: Three types of segmental lining. (a) Uniform rings. (b) Straight-jointed rings. (c) Stagger-jointed rings.

3. Experiment Results and Analysis

The experimental results of the segmental linings are converted into the corresponding prototype segmental lining according to the general law of similarity of the model test. Also, the weights applied on the vault are converted to line load along the width of the lining.

3.1. Transverse Deformation Characteristic. Figure 13 shows the deformation results in several loading stages, and the deformed shapes are reproduced through the measured radial displacement of the representative points of the middle ring, from which it can be seen that both the uniform rings and the straight-jointed rings deformed symmetrically while the stagger-jointed rings were not. Besides, the largest deformation occurs in the vault of the three types of segmental linings and the horizontal diameter is the second. However, the position at 135° of stagger-jointed rings also shows relatively large deformation, which may be attributed to the key segment of the middle ring tilted to the right side.

In the model tests, the displacement towards the outside of the tunnel is defined as positive, and in contrast, the displacement towards the inside of the tunnel is defined as negative. It can be seen from Figure 14 that for these three types of segmental lining structure, the vertical and horizontal diameter variation increases almost linearly as the concentrated load increases at the initial loading process. The value of the horizontal and vertical displacement is small, and there is no obvious elliptic deformation for the lining structures, which indicates that the segmental lining structures are in the elastic stage.

However, after the linear stage, the behaviour of different segmental linings has diverged. For the uniform rings, after the concentrated load increases linear to 550 kN/m, the displacement increased with a slight acceleration. Finally, when the concentrated load reached 594 kN/m, the vertical and horizontal diameter variation increased sharply and collapsed quickly, which showed brittle failure characteristics. As for the straight-jointed rings and stagger-jointed rings, the displacement still increased with an approximately linear slope after the linear stage, but there is an obvious acceleration trend in the increase rate. Meanwhile, the lining structure exhibited obvious elliptic deformation. In the end, the straight-jointed rings and stagger-jointed rings collapsed as the concentrated load reached 280 kN/m and 419 kN/m, respectively. In fact, it should be added that the horizontal and vertical displacement of the model test may be larger than practical engineering for the lateral confinement was not considered and imposed in the model.

3.2. Failure of the Lining Structure. It can be seen from Figure 15 that the failure modes of segmental linings have different characteristics for different assembly conditions. For the uniform rings, the deformation was small until four main cracks started to emerge at the lining hance, vault, and the bottom of the arc. The cracks at the lining vault and the bottom of the arc of each ring were consecutive in the longitudinal direction while the cracks at the hance were not, which was possibly caused by the assembly error or the existing defects of lining material. Then, the cracks expanded rapidly and caused the exposure of the circumferential wires embedded in the segments. As the loading continued to increase, the exposed reinforcement wires also broke and the whole lining structure collapsed all of a sudden.

For the straight-jointed rings, the first observed longitudinal crack emerged at the outer surface of the circumferential joint at the lining hance. As the load increased, the crack expanded quickly and more cracks appeared at the inner surface at the vault and arc bottom. After that, the cracks penetrated the circumferential joints, and the lining structure finally collapsed.

For the stagger-jointed rings, cracks also firstly emerged at the circumferential joint. However, because the distribution of the circumferential joints between the adjacent ring is different, cracks were not consecutive in the longitudinal direction. Besides, the rotation angle of circumferential joints was apparently larger than that of adjacent segments. Therefore, the deformed shapes of the adjacent rings were different, which caused obvious dislocations between the adjacent rings and the longitudinal bolts to undergo shear fracture.

3.3. Transverse Bending Rigidity Ratio. According to the experiment results of various segmental rings conducted by Huang et al. [22] and Ye et al. [23], the transverse bending rigidity ratio can be determined by comparing the variation value of the horizontal or vertical diameter of different segmental rings under the same loading condition. The calculation definition of η can be expressed as follows:

$$\begin{cases} \eta_1 = \dfrac{\Delta D_{hy}}{\Delta D_{hp}}, \\ \eta_2 = \dfrac{\Delta D_{vy}}{\Delta D_{vp}}, \end{cases} \tag{4}$$

$$\eta = \frac{EI^*}{EI} = \frac{\Delta D_2}{\Delta D_1}, \tag{5}$$

where EI and EI^* are the transverse bending rigidities of the uniform rings and the assembled segmental rings, respectively, and ΔD_1 and ΔD_2 are the maximum diameter variation values (including horizontal diameter and vertical diameter) of the assembled segmental rings and the uniform rings, respectively.

According to the definition, the value of η of the segmental linings can be calculated under each loading stage. The curves of the transverse bending rigidity ratio during loading are shown in Figure 16. As shown in Figure 16, for the straight-jointed rings, when the concentrated load is less than 176 kN/m, the calculated value of the transverse bending rigidity ratio η is fluctuating between 0.503 and 0.642, and a slight upward trend can be observed at the same time. When the concentrated load increases to 202 kN/m, which is corresponding to the cracking loading in the aforementioned failure process of the straight-jointed rings,

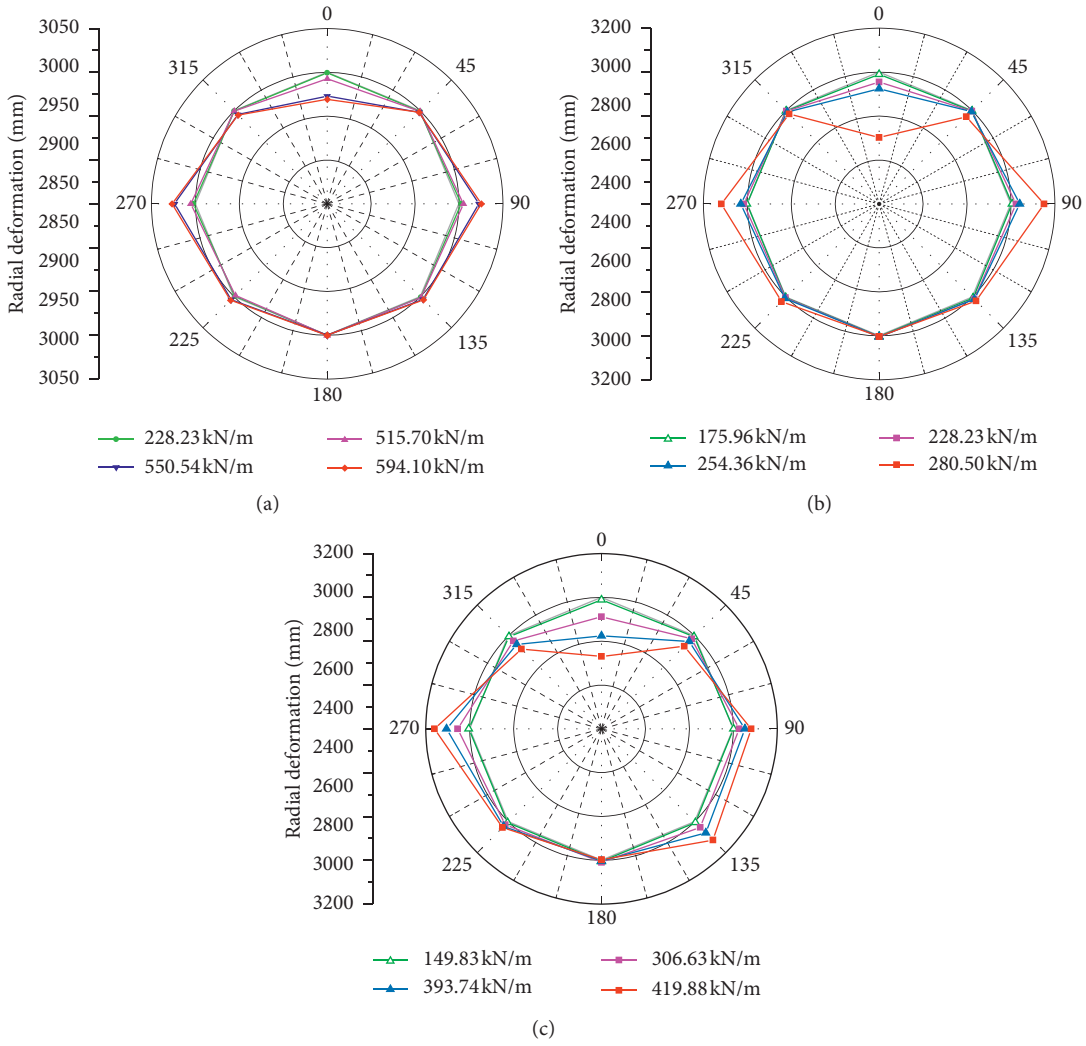

Figure 13: The deformed shape of lining models. (a) Uniform rings. (b) Straight-jointed rings. (c) Stagger-jointed rings.

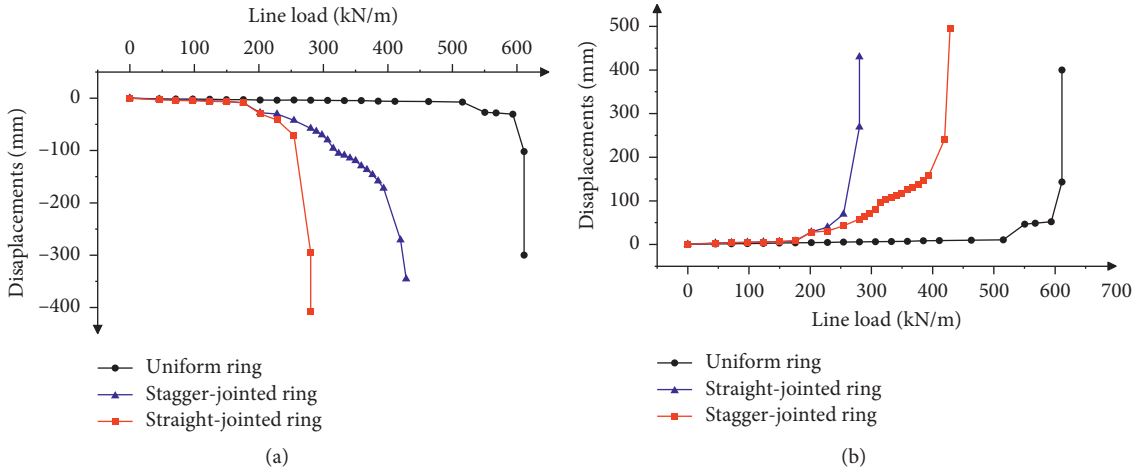

Figure 14: Variation of diameters of the target ring with the increase of the concentrated load. (a) Vertical diameters. (b) Horizontal diameters.

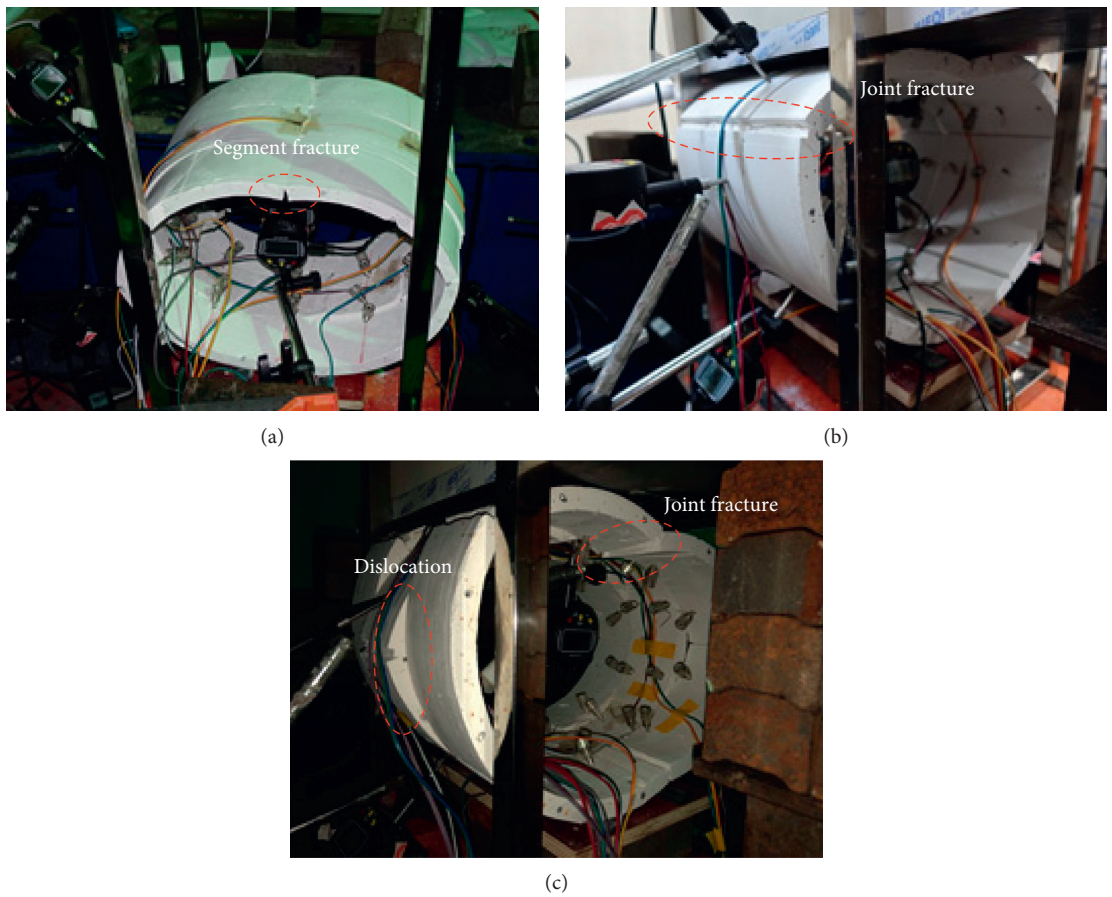

Figure 15: Failure of the lining structure. (a) Uniform rings. (b) Straight-jointed rings. (c) Stagger-jointed rings.

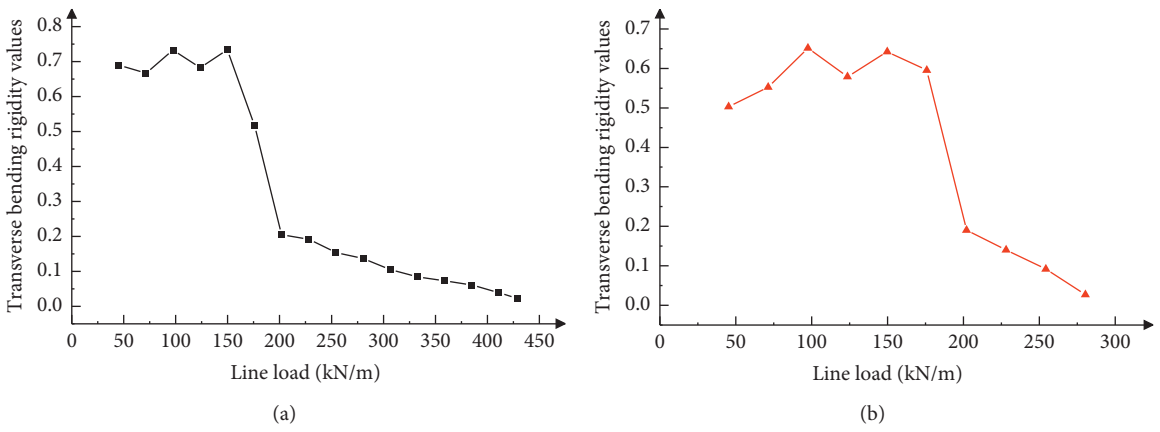

Figure 16: Relationship of the value of η and the line load. (a) Stagger-jointed rings. (b) Straight-jointed rings.

η decreases sharply to 0.190. When the concentrated load continued to increase to 280 kN/m, the decline rate of η slows down and the value of η decreases from 0.190 to 0.027. For the stagger-jointed rings, the relationship between the transverse bending rigidity ratio and loading condition is similar to that of the straight-jointed rings. When the concentrated load is less than 150 kN/m, the calculated value of the transverse bending rigidity ratio η is fluctuating between 0.667 and 0.734, and a slight upward trend can be observed. When the concentrated load increases to 202 kN/m, which is also corresponding to the cracking process of stagger-jointed rings mentioned above, η decreases sharply to 0.204. When the concentrated load is greater than 202 kN/m, the value of η descends relatively slowly from 0.191 at 228 kN/m to 0.022 at 428 kN/m.

To summarize, the stagger-jointed rings have a larger overall transverse rigidity than that of the straight-jointed rings. Before the transverse bending rigidity sharply

decreases, the average value of η of the stagger-jointed rings is 0.701 and the average value of η of the straight-jointed rings is 0.587. The variation trends in the η value of both assembled conditions are basically the same.

3.4. Regression Analysis. It is worth considering that the loading condition applied to the lining structure on the tests is different from the actual loading condition because of the surrounding soil pressure. However, the loading condition is varied under complicated stratum condition in the actual shield tunnel engineering. Therefore, it will be more meaningful to establish the relationship between the transverse bending rigidity ratio and the deformation characteristic quantity of segmental linings. Moreover, in the engineering practice, the deformation parameters are often adapted as the key performance indicators (KPIs) for evaluation of the serviceability and structural safety [35]. For instance, the ratio of convergence of horizontal diameter over the initial outer diameter, i.e., $(\Delta D/D_{\text{out}})$, is commonly regarded as the KPI. Therefore, considering that the experiment results reveal the transverse bending rigidity ratio is dependent on the deformation of tunnel lining, the relationship between the transverse bending rigidity ratio and the horizontal convergence to diameter ratio $(\Delta D/D_{\text{out}})$ is obtained by regression analysis, as shown in Figure 17.

For the stagger-jointed rings, the regression equation is

$$\eta = \begin{cases} 0.70, & \text{when } \dfrac{\Delta D}{D_{\text{out}}} < 1.00‰, \\ 0.719\left(\dfrac{\Delta D}{D_{\text{out}}}\right)^{-0.785}, & \text{when } \dfrac{\Delta D}{D_{\text{out}}} > 1.00‰. \end{cases} \quad (6)$$

For the straight-jointed rings, the regression equation is

$$\eta = \begin{cases} 0.59, & \text{when } \dfrac{\Delta D}{D_{\text{out}}} < 1.35‰, \\ 0.773\left(\dfrac{\Delta D}{D_{\text{out}}}\right)^{-0.872}, & \text{when } \dfrac{\Delta D}{D_{\text{out}}} > 1.35‰. \end{cases} \quad (7)$$

Accordingly, the variation of the transverse bending rigidity ratio could be divided into two stages, and the convergence to diameter ratio $(\Delta D/D_{\text{out}})$ of turning points is defined as the critical diameter convergence $(\Delta D/D_{\text{out}})_{\text{cr}}$, the values of which are 1.00‰ and 1.35‰ for the stagger-jointed rings and straight-jointed rings, respectively. Because of the effect of surrounding soil pressure and the lateral restriction, the value of the $(\Delta D/D_{\text{out}})_{\text{cr}}$ will possibly increase.

The formulas proposed can be valuable guidance for the evaluation of shield tunnel serviceability and safety, especially for the operated shield tunnel whose diameter convergence is larger than the critical diameter convergence. For example, according to a case study of operated shield tunnel subjected to an extreme surcharge, the field measurement results showed that the convergence to diameter ratio $(\Delta D/D_{\text{out}})$ of lower line tunnel and the upper line is on average at 6.88‰ and 25.8‰, respectively [35]. Meanwhile, another case study [36], which researches the response of the Taipei Rapid Transit System shield tunnel induced by adjacent excavation, presents that the diameter convergence of the lining structure is 4.26‰ in the horizontal direction and 7.38‰ in the vertical direction. Therefore, it can be deduced that the diameter convergences of tunnel lining in both cases have far exceeded the critical diameter convergence $(\Delta D/D_{\text{out}})_{\text{cr}}$ and consequently the transverse bending rigidity of the operated shield tunnel lining has possibly declined sharply. In the next section, another engineering case involving an operated tunnel that was also subjected to surcharges will be discussed. Besides, the relationship between the transverse bending rigidity ratio and the horizontal convergence to diameter ratio based on the experimental results will be applied to numerical analysis.

4. Case Study of an Operated Shield Tunnel and the Numerical Analysis Based on the Experimental Results

The operated shield tunnel, one of the sections of Guangzhou Metro Line 3, was once subjected to accidental surface surcharges, and relatively large diameter convergences of the segmental linings were measured. However, a foundation pit that is close to the tunnel will be excavated and the effect of the adjacent excavation is urgent to be predicted. In Sections 4.1 and 4.2, an overview of the operated tunnel and the upcoming adjacent excavation will be firstly illustrated.

Meanwhile, based on the experimental result, the transverse bending rigidity ratio η of the shield tunnel is dependent on the diameter convergence $\Delta D/D_{\text{out}}$. When diameter convergences $\Delta D/D_{\text{out}}$ are relatively large and especially exceed the critical diameter convergence $(\Delta D/D_{\text{out}})_{\text{cr}}$, the value of η decreases rapidly. To consider the exiting horizontal diameter convergence which can be obtained by on-site measurement, regression equations (6) and (7) based on the model test are employed to determine the value of the key parameter η. Moreover, a practical method was put forward to consider the variation of the parameter η and numerically predict the further deformation of the operated shield tunnel.

The specific deformation prediction method which considers the existing deformation of tunnel linings is illustrated as follows. On the one hand, the existing diameter convergence of tunnel linings can be obtained by the way of on-site measurement, so that the transverse bending rigidity ratio η_0 of operated shield tunnel can be determined through substituting the measured horizontal convergence into regression equations (6) and (7). Then, η_0 is introduced into the first excavation step of numerical model as the original value of the transverse bending rigidity ratio. On the other hand, the numerically calculated results of horizontal diameter convergence in each excavation step can be used to back-calculate the transverse bending rigidity ratio and then adopted as the original transverse bending rigidity ratio for the next excavation step. After several iterations, a final transverse

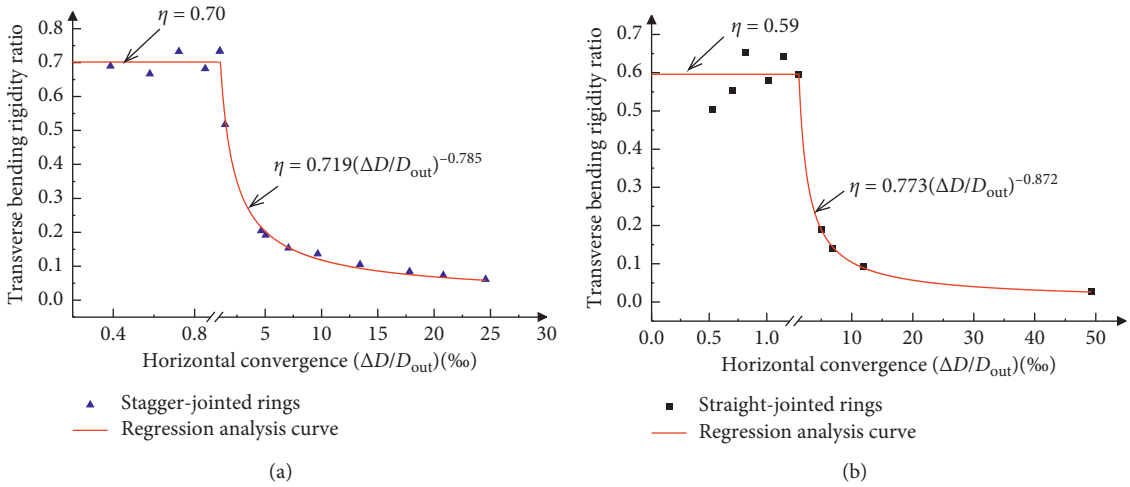

Figure 17: Regression analysis result. (a) Stagger-jointed rings. (b) Straight-jointed rings.

deformation $\Delta D/D_{out}$ is obtained as a prediction. The flowchart for the proposed prediction process of the operated shield tunnel's transverse deformation is shown in Figure 18.

4.1. Surcharge History of Shield Tunnel. A brief overview of the operated shield tunnel is described as follows. The lining structures' cross section is the same as that exhibited in Section 2.2, and the lining structure is assembled with a stagger-jointed condition. The buried depth of the tunnel crown varies from 6 m to 9 m. The soil layer at the construction site mainly includes surface fill (layer ①), medium-coarse sand (layer ②), silty clay (layer ③), hard plastic sandy clay (layer ④), plastic sandy clay (layer ④m), fully weathered granite (layer ⑤), and strongly weathered granite (layer ⑥) (see Figure 19).

The shield-driven tunnel was completed in June 2006, and after that, two accidental surface surcharges occurred. On 18 January 2013, a large amount of waste soil from a nearby construction site was piled up on the ground surface above the tunnel, and the height of the waste soils was on average 4 m. The abnormal settlement of the tunnel caused by surcharge was quickly monitored, and the waste soil was removed in two days. Figure 20(a) shows the settlement curve of the tunnel beneath the surcharged area. It can be seen that the maximum settlement of tunnel was 20.40 mm, and the settlement of the tunnel rebounded 4~9 mm after the overloading was removed. Another accidental surcharge happened on 8 December 2018, and more of the waste soil was abandoned on almost the same area and the height of the waste soils was up to 6 m. Similarly, the overloading was carried away after the sudden increase in displacement was monitored. Figure 20(b) shows the curve of the tunnel settlement after the second surcharge. It can be seen that at the overlapping area of two surcharging, the maximum settlement increased to 27.98 mm.

On 1 January 2019, the FARO three-dimensional laser scanning technique was used to measure the configuration of the segment rings that were seriously affected by the surcharging accidents. Figure 21 shows the variation of the segment rings' horizontal diameter from mileage ZDK18 + 604~ZDK18 + 754. As shown in Figure 21, the diameter convergence of segment rings was significantly increased after two surcharging accidents, and the maximum horizontal diameter convergence reaches 8.85‰ at No. 50 segment ring.

4.2. Adjacent Excavation Project. In 2019, high-rise buildings adjacent to the shield tunnel were planned and designed, and a five-level basement on the site was needed to construct. The plan view is shown in Figure 22, and the profile of section A-A is shown in Figure 23. It can be seen that the boundary of the excavation was an irregular polygon and was retained by a diaphragm wall in vertical and three levels of reinforced concrete struts in horizontal. One of the boundaries of the excavation is along the tunnel from the metro station, and the horizontal distance between the diaphragm wall and the tunnel approximately equals 5.2 m. The depth of the excavation is 21.55 m. The thickness of the diaphragm wall is 1.2 m. The length and the width of the cross sections of struts were varied in different positions and range from 1.0 m to 1.5 m. The foundation pit is excavated at four layers, which is followed in each level by strut installation.

4.3. Numerical Analysis. In the aforementioned on-site measurement data after the surcharging accidents, the maximum horizontal diameter convergence ratio of the tunnel lining was up to 8.85‰. It is of significance to consider the influence of the existing transverse deformation on the prospective deformation induced by adjacent excavation. Therefore, the effective transverse rigidity ratio η that was introduced to the numerical analysis was calculated by regression equation (6), and the convergence to diameter ratio ($\Delta D/D_{out}$) in equation (6) was based on the on-site measured horizontal diameter convergence ratio of the operated tunnel.

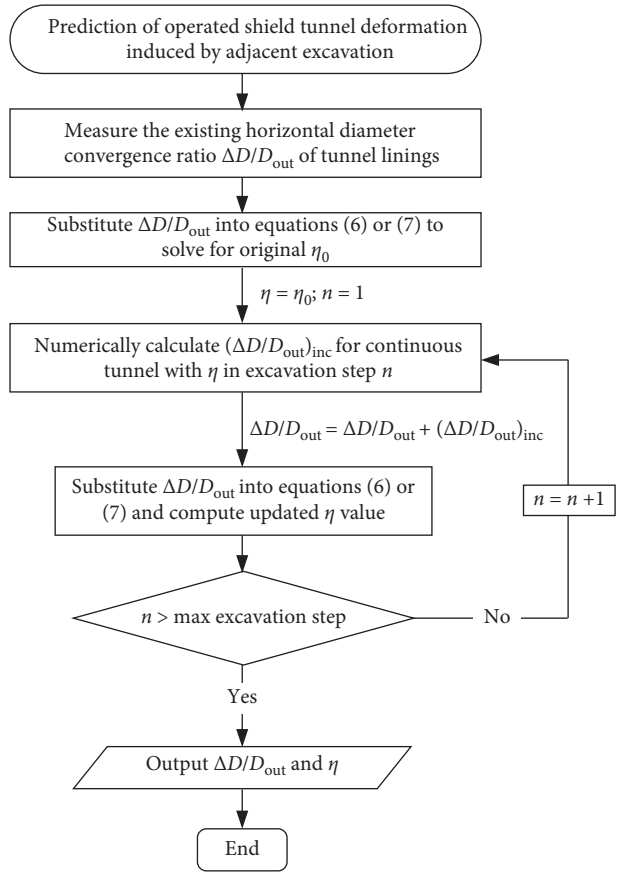

Figure 18: The flowchart of the specific deformation prediction method.

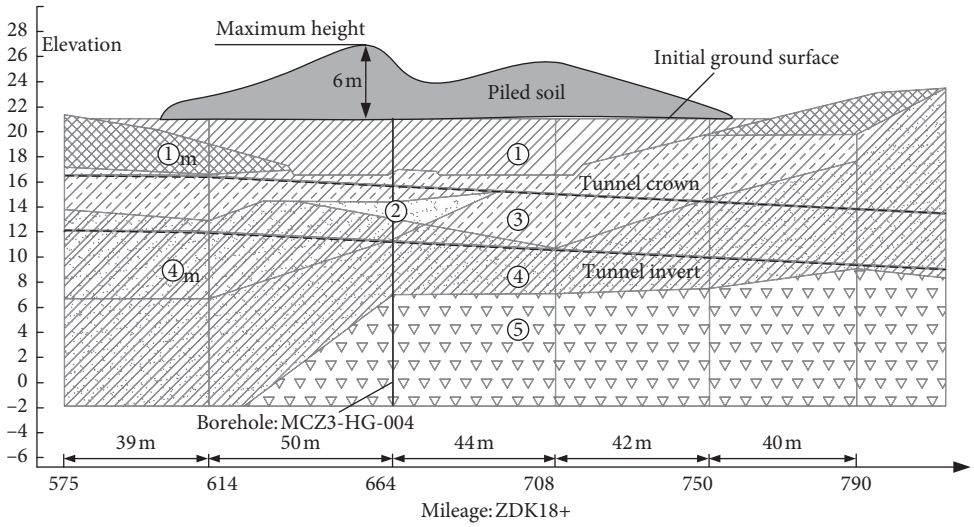

①: fill

②: medium-coarse sand

③: silty clay

④: hard plastic sandy clay

④m: plastic sandy clay

⑤: fully weathered granite

Figure 19: The detailed soil profile along the longitudinal direction.

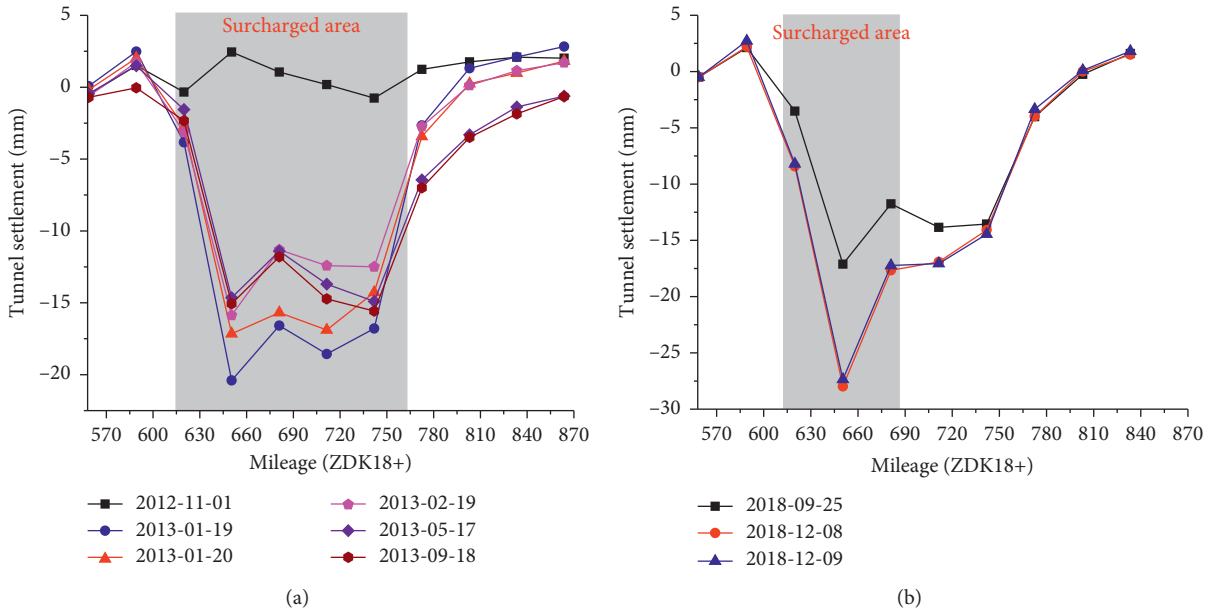

Figure 20: Tunnel settlement around the surcharged area. (a) First surcharge. (b) Second surcharge.

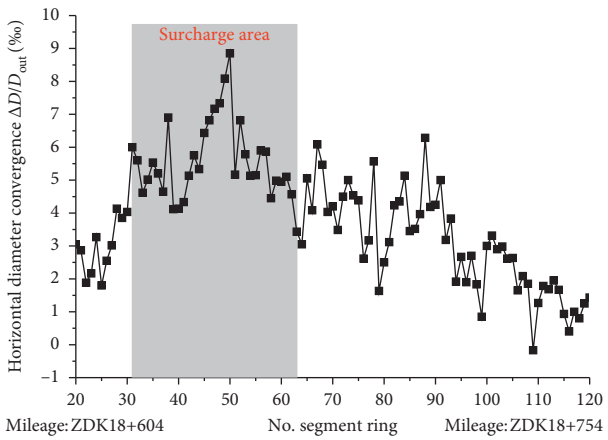

Figure 21: Diameter convergence of segment rings through on-site measurement.

Before the adjacent foundation pit was excavated, it was urgent to predict the influence of the excavation on the operated tunnel deformation. Therefore, the FEM program PLAXIS was adapted to simulate the excavation process. Considering that the surrounding environment was complicated and the concerns were mainly focused on the tunnel section that was once surcharged, the FE model based on section A-A is analysed in a plane strain condition. The domain of the model is 150 m × 60 m. Lateral boundaries are fixed in the horizontal direction and on the bottom boundary in both vertical and horizontal directions. The mesh of the FE model is shown in Figure 24.

In the model, the hardening soil model with small strain model (HSS), which can reflect the small strain behaviour of the soil [37], is used to simulate the soil. The soil parameters used in the numerical model are listed in Table 3. The diaphragm wall, struts, and tunnel lining are defined as linear material, and the elastic modulus and Poisson's ratio are 30 GPa and 0.2. The interaction between the structure and the soil is modelled with an interface element that is 0.1 m in virtual thickness. The excavation of soil layers and the installation of struts was conducted step by step. The influence of pit dewatering on the deformation of structure and soil was also simulated in the model.

In particular, for the tunnel lining under the surcharged area, the horizontal diameter convergence was up to 8.85‰, whose effective transverse rigidity ratio η can be calculated as 0.130 based on equation (6). For the purpose of studying the prospective transverse deformation of tunnel linings with different transverse rigidities, seven sets of tunnel linings with different original effective transverse rigidity ratios are involved in the numerical model, i.e., 0.7, 0.6, 0.5, 0.4, 0.3, 0.2, and 0.1, which correspond to different degrees of transverse deformation. As described in detail in Figure 18, the variation of the parameter η in each excavation step is also included in the numerical model. The transverse deformation of the tunnel linings caused by the lateral unloading in the process of adjacent excavation will result in the decline of the effective transverse rigidity ratio, which will in turn exacerbate the transverse deformation of the tunnel linings in the subsequent excavation step. The final transverse deformation states of tunnel lining are shown in Figure 25, and the variations of horizontal convergence during excavation are shown in Figure 26.

As shown in Figure 26, the horizontal convergences ΔD of the tunnel lining increase when the adjacent foundation pit is excavated from step 1 to 4, and the increment is significant from step 3 to step 4. As the original effective transverse rigidity ratio η decreases from 0.7 to 0.1, the horizontal convergences ΔD increase obviously. When the foundation pit was excavated to layer 4, the horizontal convergences ΔD increase from 12.29 mm to 27.95 mm as

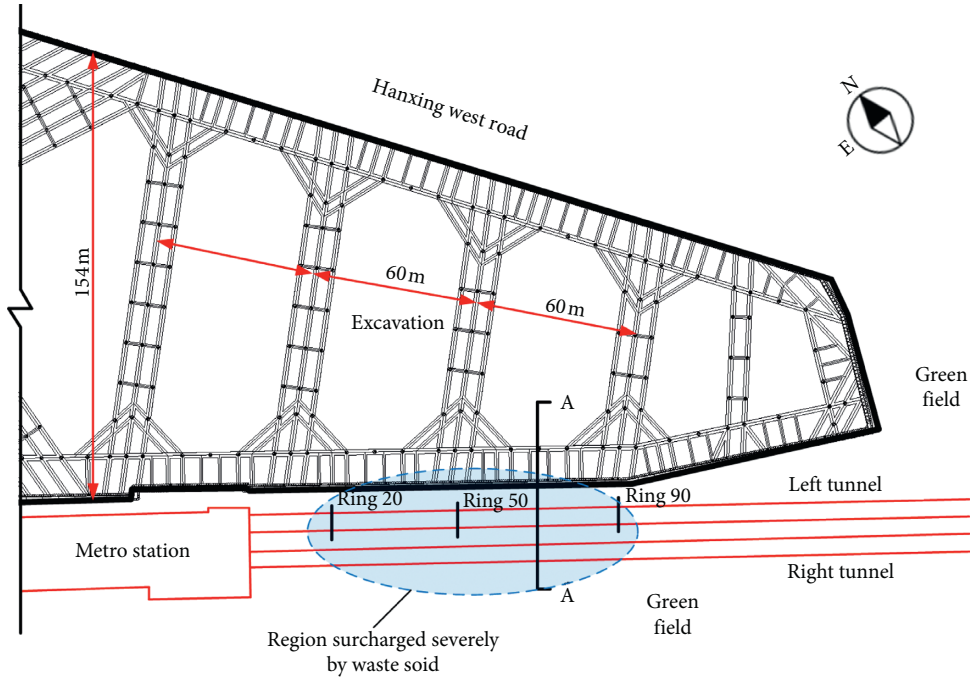

Figure 22: Plan view of the construction site.

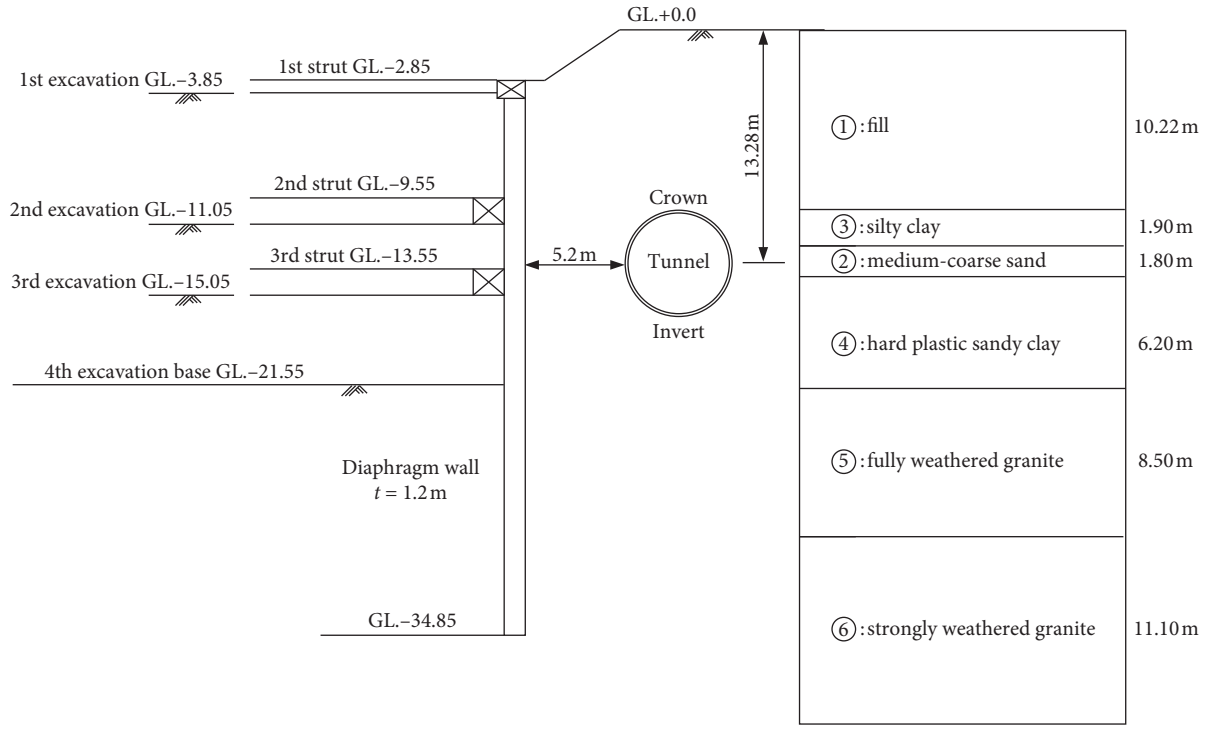

Figure 23: Profile of soil layer, excavation, and tunnel (section A-A).

the original η decreases from 0.70 to 0.1, which increases by 1.27 times. Besides, as shown in Figure 25, differing from the previous concept that regarded the effective transverse rigidity as a constant value, the final deformed shape is apparently becoming larger as the tunnel linings' original effective transverse rigidity decreases.

This indicates that the original horizontal diameter convergences of operated shield tunnel have a significant effect on the subsequent deformation induced by adjacent excavation. When the lining structure is under the same excavation stage, the lateral unloading will cause different effects on the deformation of the lining structure with

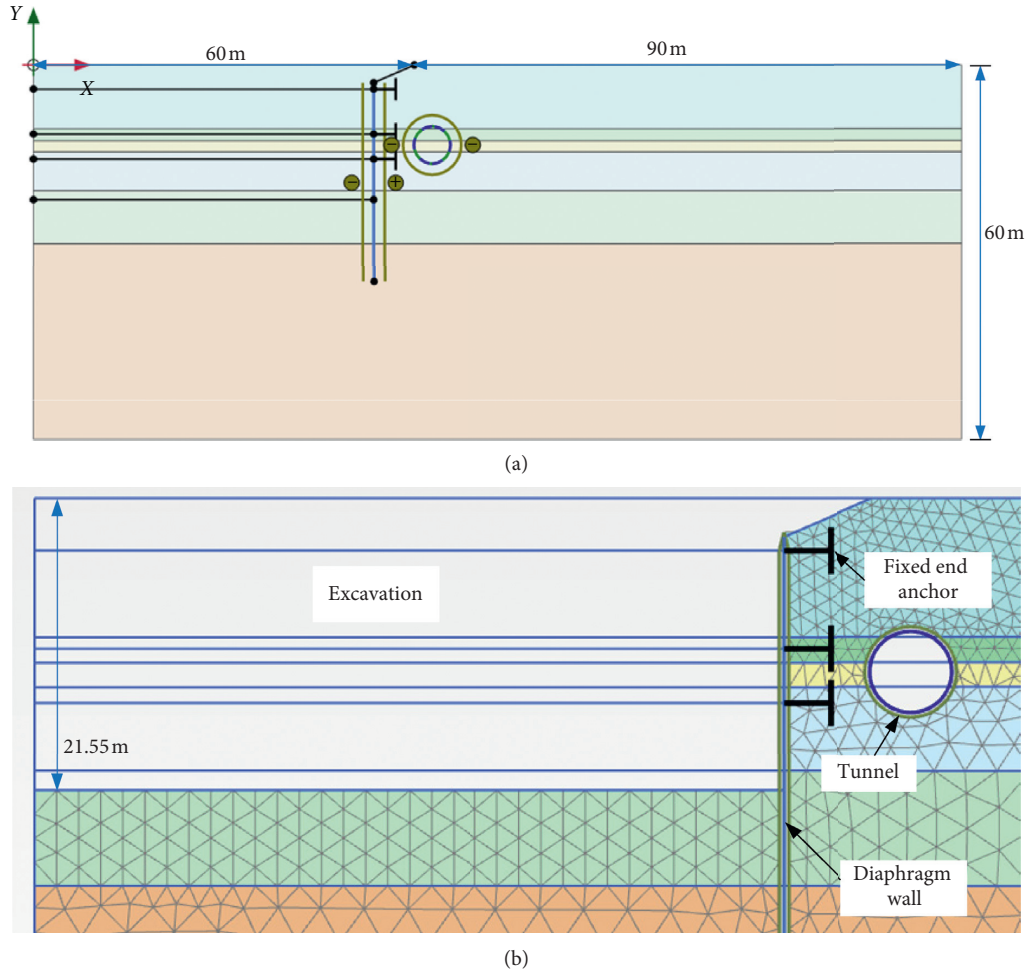

Figure 24: Finite element mesh of the simulation model.

Table 3: Input values of HSS parameters.

Soil layer type	Fill	Medium coarse sand	Silty clay	Hard plastic sandy clay	Fully weathered granite	Strongly weathered granite
γ (kN·m^{-3})	19.5	18.9	18.7	19.6	20	21
E_{oed}^{ref} (kPa)	3000	6200	6000	7500	12000	30000
E_{50}^{ref} (kPa)	4000	7500	6200	7500	12000	30000
E_{ur}^{ref} (kPa)	15000	45200	37200	47000	60000	180000
c' (kPa)	15	1	19.7	25	32	200
ϕ'	19	31	15.5	21	26	30
ψ	0	1	0	0	0	0
υ_{ur}	0.3	0.26	0.26	0.23	0.23	0.21
m	0.5	0.7	0.7	0.5	0.5	0.5
$\gamma_{0.7}$ (10^{-4})	2.0	3.0	2.0	2.0	2.0	3.2
G_0 (kPa)	30000	130600	110000	133000	180000	620000
R_f	0.9	0.9	0.9	0.9	0.9	0.9

different effective transverse rigidity ratios. With the decline of the effective transverse rigidity ratio, the horizontal convergence increases gradually and the deformation of lining structure tends to be unfavourable. Therefore, it is highly probable that the deformation results of tunnel lining will be more dangerous if a modified value of η is introduced into numerical analyses of shield tunnel-related problems.

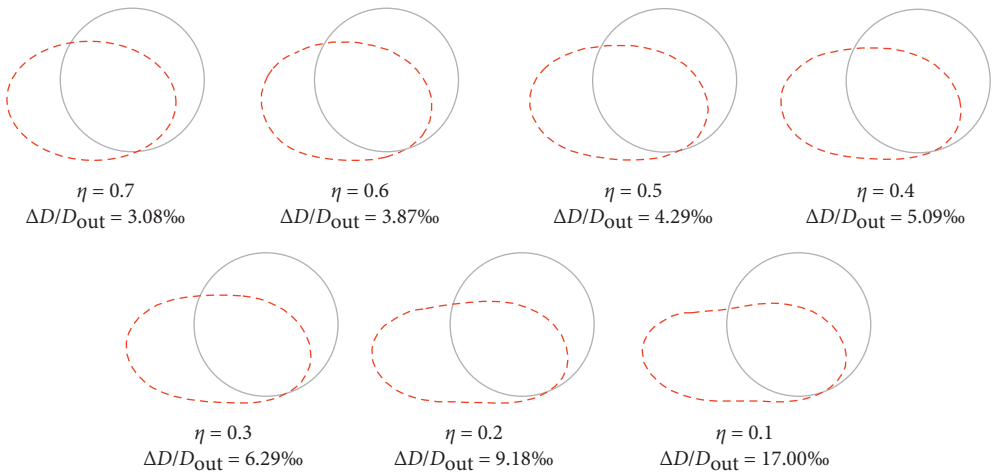

Figure 25: Final deformation state (100x magnification).

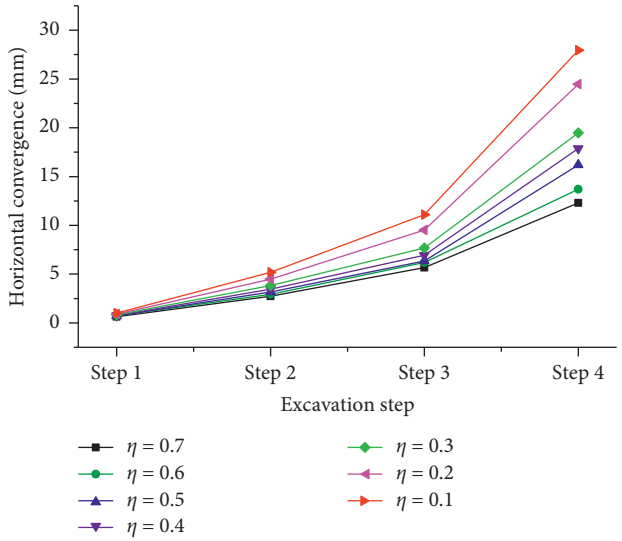

Figure 26: Horizontal convergence deformation curves of different values of η.

5. Conclusions

In this paper, experimental investigations for different assembled lining structures were first conducted to study the transverse bending rigidity, and the regression relationship between the effective transverse bending rigidity ratio and the horizontal diameter convergence was established. Besides, a case study of an operated tunnel that was once surcharged and deformed severely was presented in detail. Then, based on the regression relationship proposed from the experimental results, the influence of the transverse effective rigidity ratio on the shield tunnel's subsequent deformation induced by adjacent excavation was explored. The main conclusions can be drawn as follows:

(1) Based on the similarity theory, brittle gypsum material was used to simulate the segment concrete and featured the deformation characteristic of lining structures after the elastic stage. A detachable mould was designed for the casting of segmental rings. Hollow aluminium tubes were embedded between segmental rings to form the shape of bolts hole, through which the longitudinal joint bolts can pass. The meticulous fabrication of segmental rings revealed well the detailed structure of segmental rings.

(2) The deformation characteristic and failure process of the segmental linings are as follows: in the elastic stage, the horizontal and vertical diameter variation of three kinds of lining structure increased approximately linearly as the load increases. Cracks first appeared at the circumferential joints for both of the straight-jointed rings and the stagger-jointed rings. Finally, the fractures at the circumferential joints resulted in the collapse of lining structures. Besides, obvious dislocations between the adjacent rings occurred in the flattening deformation process of stagger-jointed rings.

(3) The model test results show that before the model cracked, the values of the transverse bending rigidity ratio η fluctuate between 0.503 and 0.642 for the straight-jointed rings and 0.667 and 0.734 for the stagger-jointed rings. But the values of η decrease sharply when the ratio of horizontal diameter convergence exceeds the critical value.

(4) Existing transverse deformation will cause the decline of transverse stiffness of operated tunnel lining and subsequently result in much unfavourable transverse deformation when subjected to lateral unloading caused by adjacent excavation. It is highly suggested to introduce the modified value of η, which is obtained through substituting on-site measurement data of the tunnel diameter convergence into the regression equation summarized from experimental results, into the numerical analyses of underground shield-driven tunnel problems so that the tunnel deformation and the lining structure safety can be predicted more precisely.

Data Availability

The data used to support the findings of this study are included within the article.

Conflicts of Interest

The authors declare that there are no conflicts of interest regarding the publication of this paper.

Acknowledgments

The authors would like to acknowledge the support from the National Natural Science Foundation of China (grant nos. 51678248 and 51878296), Independent Research Program of State Key Laboratory of Subtropical Building Science (grant no. 2017KB15), South China University of Technology, and Open Research Fund of State Key Laboratory of Simulation and Regulation of Water Cycle in River Basin (grant no. IWHR-SKL-KF201818).

References

[1] R. Chen, F. Meng, Z. Li, Y. Ye, and J. Ye, "Investigation of response of metro tunnels due to adjacent large excavation and protective measures in soft soils," *Tunnelling and Underground Space Technology*, vol. 58, pp. 224–235, 2016.

[2] W. C. Chen, Z. P. Song, W. Tian, and Z. F. Wang, "Shield tunnel uplift and deformation characterisation: a case study from Zhengzhou metro," *Tunnelling and Underground Space Technology*, vol. 79, pp. 83–95, 2018.

[3] T.-j. Liu, S.-w. Chen, and H.-y. Liu, "Deformation characterisation and distress diagnosis of a metro shield tunnel by adjacent constructions," *Advances in Civil Engineering*, vol. 2020, Article ID 4216349, 17 pages, 2020.

[4] ITA, "Guidelines for the design of shield tunnel lining," *Tunnelling and Underground Space Technology*, vol. 15, pp. 303–331, 2000.

[5] K. M. Lee, X. Y. Hou, X. W. Ge, and Y. Tang, "An analytical solution for a jointed shield-driven tunnel lining," *International Journal for Numerical and Analytical Methods in Geomechanics*, vol. 25, no. 4, pp. 365–390, 2001.

[6] H. Yu, C. Cai, A. Bobet, X. Zhao, and Y. Yuan, "Analytical solution for longitudinal bending stiffness of shield tunnels," *Tunnelling and Underground Space Technology*, vol. 83, pp. 27–34, 2019.

[7] S.-M. Liao, F.-L. Peng, and S.-L. Shen, "Analysis of shearing effect on tunnel induced by load transfer along longitudinal direction," *Tunnelling and Underground Space Technology*, vol. 23, no. 4, pp. 421–430, 2008.

[8] H. D. Morgan, "A contribution to the analysis of stress in a circular tunnel," *Géotechnique*, vol. 11, no. 1, pp. 37–46, 1961.

[9] R. B. Peck, A. J. Hendron, and B. Mohraz, "State of the art of soft-ground tunneling," *North American Rapid Excavation & Tunneling Conference Proceedings*, vol. 1, 1972.

[10] A. M. M. Wood, "The circular tunnel in elastic ground," *Géotechnique*, vol. 25, no. 1, pp. 115–127, 1975.

[11] Y. Koyama, "Present status and technology of shield tunneling method in Japan," *Tunnelling and Underground Space Technology*, vol. 18, no. 2-3, pp. 145–159, 2003.

[12] JSCE, *The Design and Construction of Underground Structures*, JSCE, Tokyo, Japan, in Japanese, 1977.

[13] Y. Tang, "The mechanism study of the staggering assembly of shield-driven tunnel," M.Phil. thesis, Tongji University, Shanghai, China, 1988.

[14] H. H. Zhu and L. B. Tao, "Study on two beam-spring models for the numerical analysis of segments in shield tunnel," *Rock and Soil Mechanics*, vol. 19, no. 2, pp. 26–32, 1998, in Chinese.

[15] Y. Koyama and T. Nishimura, "The design of lining segment of shield tunnel using a beam-spring model," *Quarterly Reports RTRI*, vol. 39, no. 1, pp. 23–27, 1998.

[16] X. Hu, Z. Zhang, and L. Teng, "An analytical method for internal forces in DOT shield-driven tunnel," *Tunnelling and Underground Space Technology*, vol. 24, no. 6, pp. 675–688, 2009.

[17] Z. Guan, T. Deng, G. Wang, and Y. Jiang, "Studies on the key parameters in segmental lining design," *Journal of Rock Mechanics and Geotechnical Engineering*, vol. 7, no. 6, pp. 674–683, 2015.

[18] W. Ding, Z. Yue, L. Tham, H. Zhu, C. Lee, and T. Hashimoto, "Analysis of shield tunnel," *International Journal for Numerical and Analytical Methods in Geomechanics*, vol. 28, no. 1, p. 57e91, 2004.

[19] J. H. Liu and X. Y. Hou, *Shield-Driven Tunnels*, China Railway Press, Beijing, China, 1991, in Chinese.

[20] X. C. Zhong, W. Zhu, Y. P. Ji, and Y. Xu, "The method to confirm the effective bending stiffness of shield-driven tunnel lining," *Geology and Prospecting*, vol. 39, no. 2, pp. 185–189, 2003, in Chinese.

[21] L. Xu, "Study on the longitudinal settlement of shield tunnel in soft soil," D.Phil. thesis, Tongji University, Shanghai, China, 2005.

[22] H. W. Huang, L. Xu, J. L. Yan, and Z. K. Yu, "Study on transverse effective rigidity ratio of shield tunnels," *Chinese Journal of Geotechnical Engineering*, vol. 28, no. 1, pp. 11–18, 2006, in Chinese.

[23] F. Ye, C.-f. Gou, H.-d. Sun, Y.-p. Liu, Y.-x. Xia, and Z. Zhou, "Model test study on effective ratio of segment transverse bending rigidity of shield tunnel," *Tunnelling and Underground Space Technology*, vol. 41, pp. 193–205, 2014.

[24] G. Zheng, Y. Lei, T. Cui et al., "Experimental research on the transverse effective bending rigidity of shield tunnels," Advances in Civil Engineering, vol. 2019, Article ID 2174562, 17 pages, 2019.

[25] X. Li, B. Huang, and Z. Yang, "Lateral equivalent stiffness of large diameter shield tunnel lining structure at various buried depths," *Journal of Tongji University*, vol. 43, no. 8, pp. 1159–1166, 2015.

[26] K. Feng, C. He, and S. L. Xia, "Prototype tests on effective bending rigidity ratios of segmental lining structure for shield tunnel with large cross-section," *Chinese Journal of Geotechnical Engineering*, vol. 33, no. 11, pp. 1750–1758, 2011, in Chinese.

[27] K. Uchida, "Design and engineering of large bore slurry shield tunnel lining system for trans-Tokyo bay highway," *Civil Engineering in Japan*, vol. 30, pp. 54–67, 1992.

[28] Y. Kashima, N. Kondo, and M. Inoue, "Development and application of the DPLEX shield method: results of experiments using shield and segment models and application of the method in tunnel construction," *Tunnelling and Underground Space Technology*, vol. 11, no. 1, pp. 45–50, 1996.

[29] G. Zheng, J. Pan, Y. Li, X. Cheng, and X. Li, "Deformation and protection of existing tunnels at an oblique intersection angle to an excavation," *International Journal of Geomechanics*, vol. 20, no. 8, Article ID 05020004, 2020.

[30] S. M. Wang, Q. Y Yu, S. W. Duann, and B. Peng, "A model test for the progressive failure mechanism of lining segment structure of underwater shield tunnels," *China Civil Engineering*, vol. 4, pp. 111–120, 2016, in Chinese.

[31] C. He, J. G. Zhang, and Z. Yang, "Model test study on the mechanical characteristics of segment lining for the Wuhan Yangtze river tunnel," *China Civil Engineering Journal*, vol. 41, no. 12, pp. 85–90, 2008.

[32] D. W. Huang, S. H. Zhou, X. Z. Wang, H. B. Liu, and R. L. Zhang, "Design method for longitudinal segment joints of shield tunnel model," *Chinese Journal of Geotechnical Engineering*, vol. 37, no. 6, pp. 1068–1076, 2015.

[33] S. Wang, X. Wang, B. Chen, Y. Fu, Y. Jian, and X. Lu, "Critical state analysis of instability of shield tunnel segment lining," *Tunnelling and Underground Space Technology*, vol. 96, Article ID 103180, 2020.

[34] R. Guo, M. Zhang, H. Xie, C. He, Y. Fang, and S. Wang, "Model test study of the mechanical characteristics of the lining structure for an urban deep drainage shield tunnel," *Tunnelling and Underground Space Technology*, vol. 91, Article ID 103014, 2019.

[35] H. Huang, H. Shao, D. Zhang, and F. Wang, "Deformational responses of operated shield tunnel to extreme surcharge: a case study," *Structure and Infrastructure Engineering*, vol. 13, no. 3, pp. 345–360, 2016.

[36] C.-T. Chang, C.-W. Sun, S. W. Duann, and R. N. Hwang, "Response of a Taipei rapid transit system (TRTS) tunnel to adjacent excavation," *Tunnelling and Underground Space Technology*, vol. 16, no. 3, pp. 151–158, 2001.

[37] T. Benz, R. Schwab, and P. Vermeer, "Small-strain stiffness in geotechnical analyses," *Bautechnik*, vol. 86, no. S1, pp. 16–27, 2009.